SAND2011-3730C

Improving the Quality and Spatial Resolution of Aerially-Collected Radiation Data using Spatially-Variant Deconvolution

James R Curry
Sandia National Laboratories
Albuquerque, NM

Richard J Detry*
Sandia National Laboratories
Albuquerque, NM
rdetry@sandia.gov

Kristin L. Adair
Sandia National Laboratories
Albuquerque, NM
kladair@sandia.gov

Thomas M. Weber
Sandia National Laboratories
Albuquerque, NM
tmweber@sandia.gov

*Corresponding author

Abstract

Aerial vehicles can be a convenient platform for detection equipment for rapid radiation surveys of a large area. Traditional single-element detection systems are readily available and easy to use on moving aircraft. However, an aircraft's changing altitude or variations in the terrain underneath the aircraft can dramatically vary the source-to-detector distance, leading to distortions in the measured data. Even if the terrain and flight path are flat, the images produced by uncollimated airborne detectors are blurred by the detector's altitude off the ground. Building upon and extending techniques developed to correct images collected by the flawed mirror aboard the Hubble Space Telescope (Fullton, et al. 1994), we have developed a spatially-variant deconvolution technique which has proven effective at correcting the distortions and improving the spatial resolution of aerially-collected radiation data. We will present the technique and results obtained using data collected with a sodium iodide detector flown aboard a rotary-wing aircraft. A discussion of future research directions will follow.

Introduction

Sandia National Laboratories has developed new data processing techniques for aerially collected radiation data. The techniques developed include a new deconvolution-based approach that greatly sharpens the map produced after flying a radiation scan over a scene. The authors believe that this technique can also be used as a means to estimate the activity of the sources that the detector has flown over. This paper describes the progress towards a working deconvolution algorithm for map sharpening and source activity estimation.

The traditional approach to analyzing aerially collected radiation data involves making a simple altitude correction that accounts for atmospheric attenuation but not $1/r^2$ losses caused by the variation of source to detector distance within the field of view, or footprint, of the detector. The omission of $1/r^2$ losses from these algorithms means that an assumption has been made that the emission rate is constant over the footprint of the detector and that the terrain altitude is constant over that same footprint. The detector's footprint is typically defined as being a circle of diameter equal to twice the detector's altitude above ground level. Previous aerial radiation measurement systems have always been mounted on manned fixed or rotary winged aircraft and have been designed to perform coarse

(~200m spatial resolution) surveys over large areas. If a higher degree of spatial precision is desired, we must abandon the assumptions of a fixed detector footprint and uniform terrain and emission rate within that footprint. Our goal is to eliminate these assumptions from the analysis process in order to enable higher-fidelity output as quickly as possible after the detector lands.

Sensor Description

The detector consists of a single 3”x9” scintillator crystal connected to a ruggedized photomultiplier tube (PMT). The 14-pin base on the PMT is fitted with a multichannel analyzer (MCA), which supplies the PMT high voltage and continuously produces 1024-channel spectra at a regular frequency of 1 Hz.

Also on board the detector pod is a laser rangefinder, which returns Above Ground Level (AGL) altitude, and a GPS receiver. Integrating all three sensors is a single-board computer (SBC). The 486-based SBC has no moving parts and relies on solid-state media, which is critical for reliable performance in the vibration environment aboard the helicopter. The SBC has low power requirements, which helps to minimize the weight of the entire system.

Running on the SBC are two key pieces of software: 1) Radiological Threat Search and Mapping Software (RTSMS), a Sandia-developed sensor integration software platform, and 2) PostgreSQL, an open-source relational database. RTSMS performs Ethernet communications with the MCA and serial communications with the GPS and rangefinder, logging the synchronized data in the PostgreSQL database. After the flight has ended, the data remain in the database and are easily retrieved by RTSMS upon request from an external client.

Radiation Surveys

In June of 2010, a number of flight tests were conducted to obtain data for use in development of the new signal processing algorithms discussed later in this paper. The sensor was mounted to a small, unmanned helicopter that was flown at a speed of 6 m/s with 6 meters between scan lines. Two different survey regions were used in conducting these flight tests, both at a site consisting of a long earthen dam in order to provide varying terrain:

- A 190-meter square centered over the dam, used when a single source was exposed. The source location was on top of the dam at the center of the square.
- A rectangle, 150 meters by 240 meters, nearly centered over the dam, used on background surveys and when two sources were exposed. One source was located on top of the dam and one at the bottom of the dam.

In addition to background characterization surveys, the following point-source surveys were conducted with completely uncollimated sources:

- 0.85 Ci ^{192}Ir at top of dam, flight 40 meters above dam, square survey pattern
- 0.85 Ci ^{192}Ir at top of dam, flight 60 meters above dam, square survey pattern
- 6.7 Ci ^{192}Ir at top of dam, flight 40 meters above dam, square survey pattern
- 6.7 Ci ^{192}Ir at top of dam, flight 80 meters above dam, square survey pattern

- 0.03 Ci ^{60}Co at top of dam, 0.85 Ci ^{192}Ir at bottom of dam, flight 40 meters above dam, rectangular survey pattern
- 0.03 Ci ^{60}Co at top of dam, 0.85 Ci ^{192}Ir at bottom of dam, flight 60 meters above dam, rectangular survey pattern

Spatially Variant Deconvolution

Deconvolution is expressed mathematically as the solution of

$$f * g = h + \epsilon \qquad (Equation\ 1)$$

for f, where f is the dataset to be estimated, $*$ is the convolution operator, g is the convolution kernel (in deconvolution, called the point-spread function), h is the measured data and ϵ is the error. By solving for f, we can estimate the actual data that caused the detector (represented by the point-spread function) to measure h. In terms of a radiation detection mission, f represents the actual size, shape and location of sources distributed across the area surveyed and g is a detector response model.

Deconvolution is used extensively in the fields of astronomy ((Primot, Rousset and Fontanella 1990), (Jefferies and Christou 1993), (Schulz 1993)) and medical imaging ((Seibert and Boone 1988), (Shao and Karp 1991), (Taxt 1995)). In radiation detection, deconvolution has also seen some use in attempting to improve the energy resolution of spectra collected with low-resolution detectors (Knoll 2010). Though the mining industry and the US Government have been collecting radiation data from airborne detectors for decades, our research, as far as we can tell, represents the first attempt to apply deconvolution to improve the spatial clarity of aerially collected radiation data.

Traditionally, deconvolution has been used with an invariant point-spread function. For our specific situation, this will not work because changes in the AGL altitude and/or terrain variations can cause dramatic changes in the response of the detector to sources that might be present on the ground. In order to properly handle this fact and accurately reconstruct the source distribution on the ground, we must use a spatially variant point-spread function. This means that for each location of the detector during the flight, we will compute a different point-spread function. We term deconvolution performed with this type of point-spread function *spatially variant deconvolution*.

Probably owing to the amount of computational power required to solve the problem, the scientific literature contains relatively few examples of spatially variant deconvolution. One example dates back to the early 1990s, when it was discovered that the Hubble Space Telescope (HST) had been launched with a flawed mirror. In (Fullton, et al. 1994), the authors describe a spatially variant deconvolution technique for correcting images from the HST. However, this technique divides the image into regions which each share relatively uniform distortions due to the flawed mirror. The individual regions are each deconvolved with their own invariant point-spread functions, and then the deconvolved images are stitched back together. For aerially-collected radiation data this approach might work for very simple terrain and flight patterns, but in order to be generally useful a more generalized spatially variant point-spread function is needed.

Our approach to this generalized spatially variant deconvolution problem is to first develop a detector response model. We then use this model to build a spatially variant point-spread function based on the terrain measurements made during the flight. Like most airborne radiation detectors, the spectrometer used in this system is equipped with an above-ground-level (AGL) altimeter. We use this to build a model of the terrain that the detector has scanned. With a high-resolution terrain model and the detector's 3-D position and orientation coordinates from the flight, we can build the high-resolution detector response model that is not subject to the assumptions of uniform source activity or terrain elevation under the useful footprint of the detector. This detector response model then serves as the point-spread-function in a deconvolution algorithm.

Point-Spread Function Calculation

As shown in equation 2 below, the detector response model takes into account the detector's position relative to the terrain, its orientation, atmospheric attenuation and detector crystal absorption efficiency.

$$R_{det}(r, m, \phi, D, L) = \sum_{m} N(m)F(m, \phi)e^{-\alpha(m)r}\left(\frac{DL|sin\phi + \pi(D/2)^2|cos\phi|}{4\pi r^2}\right) \qquad (Equation\ 2)$$

where:

- $N(m)$ is the count rate emitted by the source at energy m
- $F(m, \phi)$ is the efficiency of the detector at energy m and incident angle ϕ
- $\alpha(m)$ is the atmospheric attenuation coefficient at energy m
- r is the source-to-detector distance
- D is the diameter of the cylindrical detector
- L is the length of the cylindrical detector

As the detector flies its mission, it measures its altitude both above ground level and above mean sea level (MSL). This enables a simple reconstruction of the ground surface using the equation:

$$terrain = MSL - AGL \qquad (Equation\ 3)$$

where MSL is a matrix containing the MSL altitude measured by the detector at every sample location and AGL is a matrix containing the AGL altitude measured by the detector at every sample location. The result of this calculation, $terrain$, is a matrix containing the MSL elevation of each point on the ground surface.

Let p be the set of n 3-dimensional sample locations visited by the detector during its flight and g be the set of n 3-dimensional points on the ground. We define the following matrix:

$$D = \begin{pmatrix} |p_1 - g_1|_2 & \cdots & |p_1 - g_n|_2 \\ \vdots & \ddots & \vdots \\ |p_n - g_1|_2 & \cdots & |p_n - g_n|_2 \end{pmatrix} \qquad (Equation\ 4)$$

where $|v|_2$ denotes the l^2-norm of some vector v. Thus, each column of the square matrix D contains a vector representing the 3-dimensional distance from a single detector location to all points on the ground. Each row of D contains a vector representing the 3-dimensional distance from a single point on the ground to each detector location. The diagonal of D contains a vector representing the AGL altitude of the detector at each detector location in p.

By evaluating equation 2 for each element of the matrix D defined in equation 4 for the energy level of each channel in the spectrum produced by the detector, we obtain a three dimensional matrix, which we term here K. The matrix K has the shape $[n \quad n \quad n_{chan}]$ where n is the number of sample locations in the survey and n_{chan} is the number of channels in the spectra collected by the detector.

K is constructed in the following manner. The first dimension of K represents all possible locations on the ground and the second dimension represents all possible locations of the detector during the survey. The third dimension of K represents all possible energy levels. Each element K_{xyz} represents the fraction of gamma particles emitted from location x that are successfully measured by the detector at location y, provided the particles are emitted with an energy of z. This is precisely the definition of the spatially variant point-spread function needed for our deconvolution problem.

We implemented and tested numerous deconvolution algorithms and found two that provide the most consistent results for our test data: Basic Iterative Deconvolution Non-negative and Maximum-Likelihood Estimation. Each of these algorithms is described below and sample results for each are provided in the Results section.

Deconvolution via Basic Iterative Deconvolution Non-negative (BID-NN)

One method of solving the deconvolution problem is an iterative method first proposed by Van Cittert (Van Cittert 1931). This method is sometimes called Basic Iterative Deconvolution, and it is formulated as follows:

$$x^{k+1} = x^k + b\left(h - x^k * g\right) \qquad (Equation\ 5)$$

where h is the measured data, g is the point-spread function, x^k is the estimate of the reconstructed original data at iteration k, and b is a constant relaxation factor which can be chosen to aid convergence. h is usually a good value for x^0.

Logically, this is a very simple algorithm. At each iteration the equation convolves the current estimate with the point-spread function, effectively asking the question "If the real data were equal to my current estimate, what would my detector measure?" The result of this convolution is subtracted from the actual measured data, computing an error value for the current estimate. This error value is scaled by the relaxation factor b, and then the estimate is corrected by the scaled error. The corrected estimate becomes the new current estimate and the process is repeated.

Since any negative values in x^k are invalid for our problem, as they would indicate "negative" radioactivity, we can enforce a non-negativity constraint on x^k at each iteration by clipping any negative

elements of x^k to zero. Basic Iterative Deconvolution with this constraint is called Positive Iterative Deconvolution or Basic Iterative Deconvolution, Non-Negative (BID-NN).

Deconvolution via Maximum-Likelihood Estimation

Another iterative method of solving the deconvolution problem is Maximum Likelihood Estimation (MLE). The most commonly used algorithm is the Richardson-Lucy MLE algorithm ((Richardson 1972), (Lucy 1974)) and it is formulated as follows:

$$x^{k+1} = cx^k \left(\frac{h}{x^k * g} * g \right) \qquad (Equation\ 6)$$

where h is the measured data, g is the point-spread function, x^k is the estimate of the reconstructed original data at iteration k, and c is a normalization constant which can be chosen to aid convergence and multiplication and division are performed point-wise.

This algorithm is similar to BID-NN in that it attempts to answer the same basic question, but it has several key differences. First, instead of the difference between the actual measured data and the estimate of the reconstructed original for calculation of the error, MLE uses the ratio of the two which is then convolved with the point spread function to convert it back to the same space as the reconstructed estimate. This algorithm requires an additional convolution step when compared to BID-NN, but this is offset by faster convergence. Second, this algorithm does not involve an additional step to maintain the positivity constraint as only multiplication and division of positive numbers occur.

Results

All of the results featured below were generated from data collected at test flights performed in June 2010 in which the flights were conducted over an earthen dam to provide varying terrain. The detector was flown in a regular grid-pattern at 6 meters per second. Scan lines were placed 6 meters apart. The dam slopes down steeply from an elevation of about 60m MSL to about 35m MSL at the bottom. Figure 1 shows the dam's terrain and the detector's elevation above this terrain.

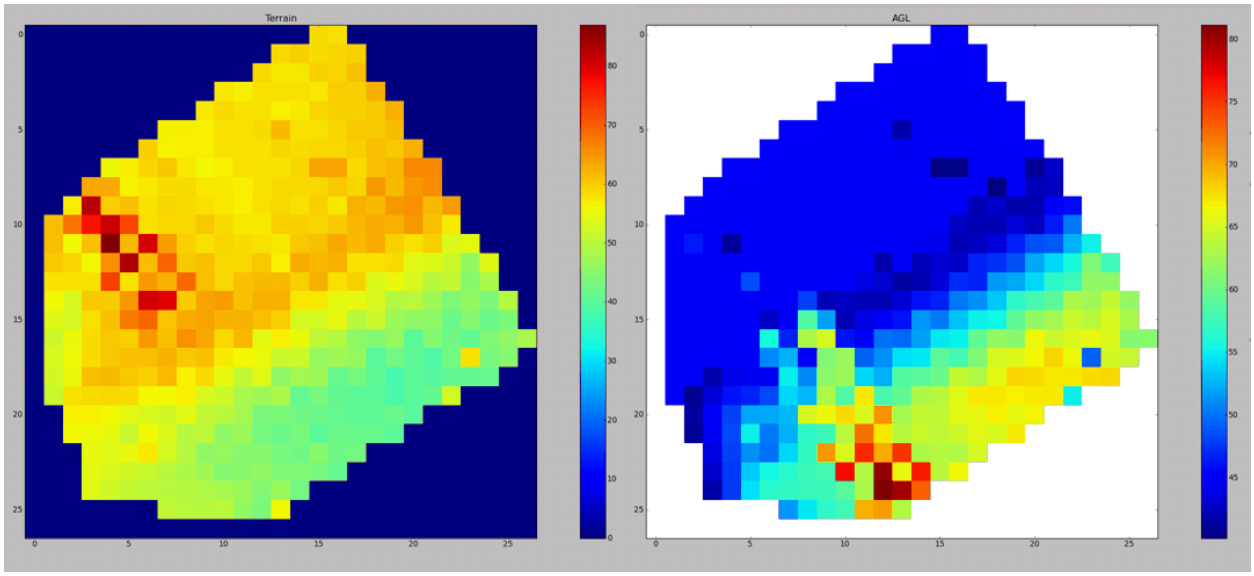

Figure 1. Terrain MSL elevation (left) and sensor AGL elevation (right)

Map Sharpening

A scan was flown over the dam with a single radiation source stationed at the top of the dam. Figure 2 shows the counts as measured and the emissions of gross counts as estimated by our BID-NN algorithm. In the measured counts map, the count rate generated by the single 0.85 Ci ^{192}Ir source results in a large diffuse area of elevated counts that highlights an area extending approximately 60 meters in all directions from the true location of the source. In the BID-NN reconstruction, the gradient is much greater and the map correctly shows that much of this ground is not contaminated.

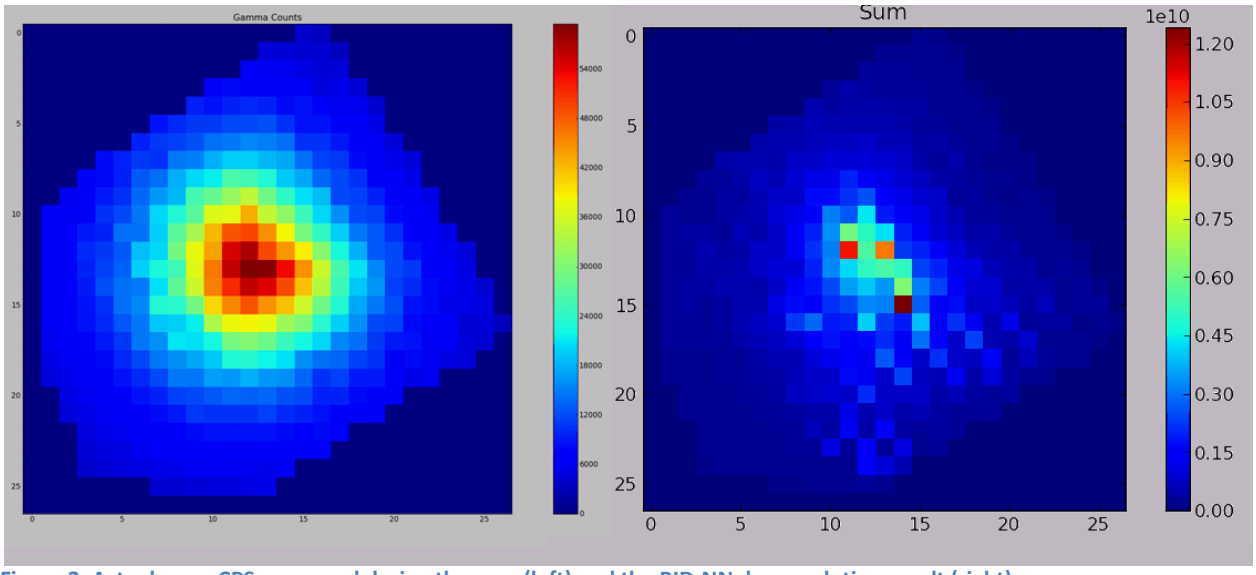

Figure 2. Actual gross CPS measured during the scan (left) and the BID-NN deconvolution result (right)

A second scan was flown over the dam when the same 0.85 Ci ^{192}Ir source was located at the bottom of the dam and a 0.03 Ci ^{60}Co source was located at the top of the dam. In the measured counts map the larger iridium source masks out the smaller cobalt source. However, the MLE deconvolution result shown in Figure 3 clearly shows the two distinct sources and correctly shows the iridium source as much larger than the cobalt source.

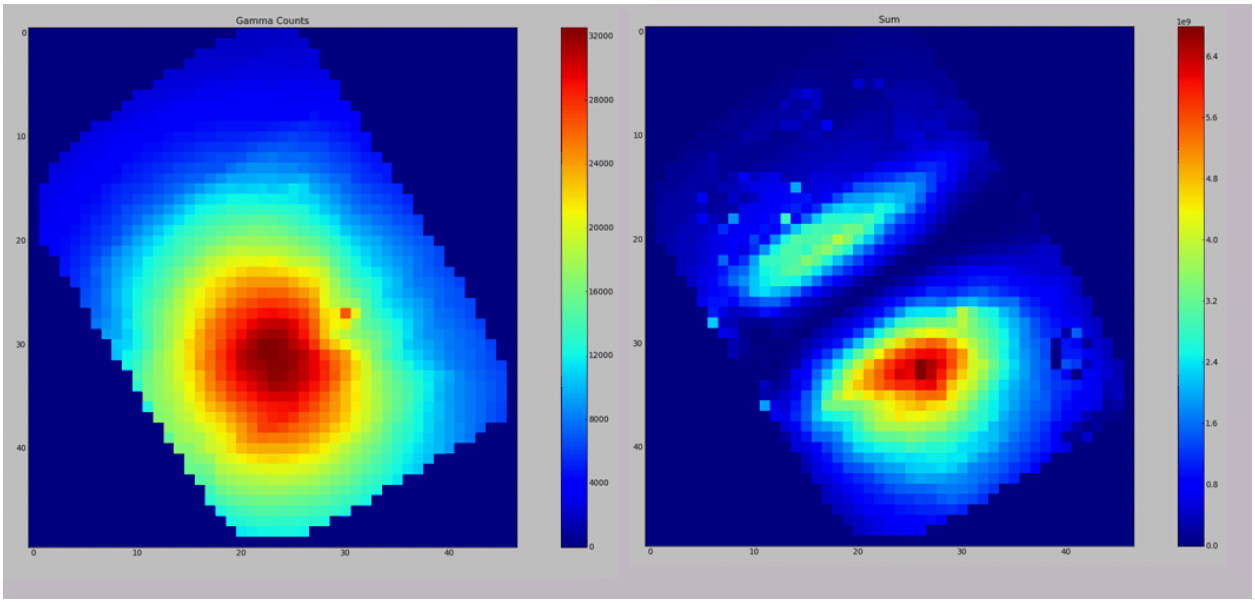

Figure 3. Measured gross counts (left) and MLE deconvolution result (right) for 2-source test configuration

Source activity estimation

We intend to refine the detector response model during 2011 and this should improve the accuracy of the source activity estimates. That said, the deconvolution technique currently under development does show promise for providing at least a rough n order-of-magnitude estimate for the activity of the source present on the ground. Figure 4 shows the reconstructed spectrum (blue dots), as compared to the theoretically predicted spectrum (red line) for the 0.85 Ci ^{192}Ir source. The theoretically predicted spectrum is a high-resolution spectrum synthetically generated using published gamma ray energies and intensities. (Online Spectrum Catalog for NaI n.d.) Note that the reconstructed spectrum includes background and the predicted emission spectrum does not; this is the source of the peaks at 1463 keV and 2614 keV in the reconstruction. The light blue line shows the measured spectrum. This plot demonstrates that the relative and absolute heights of the major ^{192}Ir peaks have been reconstructed to approximately the right order of magnitude. We expect that this spectrum will prove useful not only for isotope identification but also for providing rough estimates of quantity present of identified isotopes,

since the !peak heights (or more accurately, the peak areas) correlate to the actual source activity.

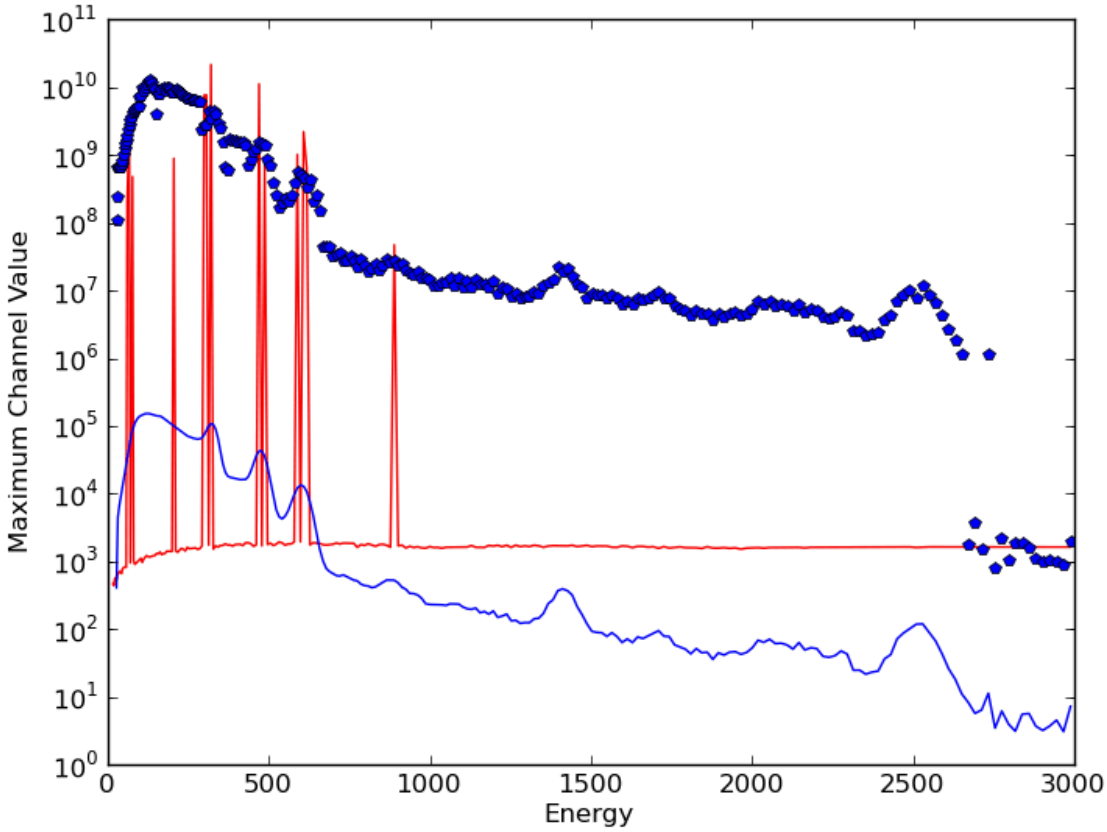

Figure 4. Reconstructed spectrum (blue dots) compared to the theoretically predicted spectrum (red line). The light blue line shows the measured spectrum

Future Work

The next major step in our work is to include Compton scattering effects in our sensor response model in a computationally efficient manner. Including these effects will improve the results of our deconvolution algorithms and lead to more accurate source location and size estimates. We also hope to conduct additional flights to obtain more data that will help us improve and characterize the algorithms and perhaps identify additional algorithms. Finally, we plan on investigating the use of an isotope identification algorithm to provide source identification.

Conclusion

Sandia National Laboratories has developed a new technique for the analysis of aerially-collected radiation data. This technique first builds a spatially-variant detector response model which takes into account the position of the detector relative to the terrain surface at each location along the flight path. This response model is then used as a point-spread function in a deconvolution routine. The output of

the deconvolution is an estimated reconstruction of the original distribution of radiation emissions on the terrain surface. The new technique has theoretical advantages over the traditional approach to analysis of aerially-collected radiation data, and sample results from a flight test event have been presented, demonstrating the technique's effectiveness. Finally, directions for future research have been presented.

Works Cited

Fullton, L. K., B. W. Carney, J. M. Coggins, K. A. Janes, N. Heasley, and P. Seitzer. "Interative/Recursive image deconvolution. Method and application to HST images." *Astronomical Data Analysis Software and Systems III*, no. 61 (1994): 288=291.

Jefferies, S. M., and J. C. Christou. "Restoration of Astronomical Images by Interative Blind Deconvolution." *The Astronomical Journal*, no. 415 (October 1993): 862-874.

Knoll, G. F. *Radiation Detection and Measurement.* John Wiley and Sons, 2010.

Lucy, L. B. "An Iterative Technique for the Rectification of Observed Distributions." *Astronomical Journal*, no. 79 (1974): 745-754.

Online Spectrum Catalog for NaI. http://www.inl.gov/gammaray/catalogs/nai/catalog_nai.shtml.

Primot, J., G. Rousset, and J. C. Fontanella. "Deconvolution from wave-front sensing: a new technique for compensating turbulence-degraded images." *Journal of the Optical Society of America* 7, no. 9 (1990): 1598-1608.

Richardson, W. H. "Bayesian-Based Iterative Method of Image Restoration." *Journal of the Optical Society of America*, no. 62 (1972): 55-59.

Schulz, T. J. "Multiframe blind deconvolution of astronomical images." *Journal of the Optical Society of America A* 10, no. 5 (1993): 1064-1073.

Seibert, J. A., and J. M. Boone. "X-ray scatter removal by deconvolution." *Medical Physics* 15, no. 4 (1988): 567-575.

Shao, L., and J. S. Karp. "Cross-plane scattering correction-point source deconvolution in PET." *IEEE Transactions on Medical Imaging* 10, no. 3 (September 1991): 234-239.

Taxt, T. "Restoration of medical ultrasound images using two-dimensional homomorphic deconvolution." *IEEE Transactions on Ultrasonics, Ferroelectrics, and Frequency Control* 42, no. 4 (July 1995): 543-554.

Van Cittert, P. H. "Zum Einfluss der Spaltbreite auf die Itensitatswerteilung in Spektrallinien 11." *Z. Phys.* 69 (1931): 298-308.